IEEE Photonics Journal
An IEEE Photonics Society Publication

Open Access

# Torsion Sensor with Rotation Direction Discrimination Based on a Pre-twisted In-Fiber Mach–Zehnder Interferometer

Volume 9, Number 3, June 2017

Zhiyong Bai
Mi Deng
Shen Liu
Zhe Zhang
JinShan Xu
Jian Tang
Ying Wang
Changrui Liao
Yiping Wang

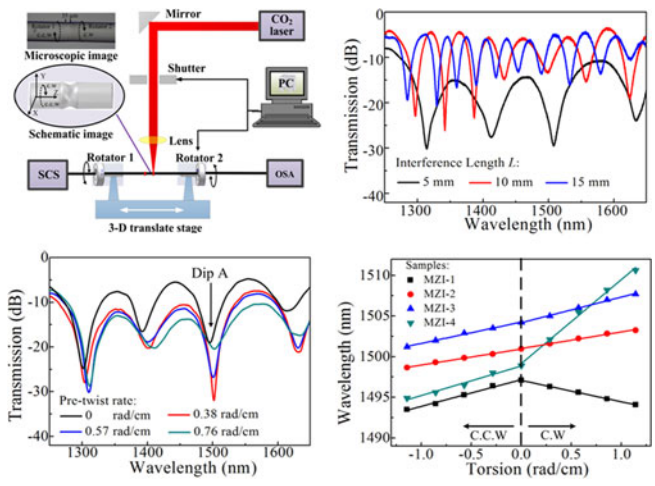


DOI: 10.1109/JPHOT.2017.2702662
1943-0655 © 2017 IEEE

# Torsion Sensor with Rotation Direction Discrimination Based on a Pre-twisted In-Fiber Mach–Zehnder Interferometer

**Zhiyong Bai, Mi Deng, Shen Liu, Zhe Zhang, JinShan Xu, Jian Tang, Ying Wang, Changrui Liao, and Yiping Wang**

Key Laboratory of Optoelectronic Devices and Systems of Ministry of Education and Guangdong Province, College of Optoelectronic Engineering, Shenzhen University, Shenzhen 518060, China

*DOI:10.1109/JPHOT.2017.2702662*


Manuscript received April 19, 2017; accepted May 5, 2017. Date of current version May 19, 2017. This work was supported in part by the National Natural Science Foundation of China under Grant 61635007, Grant 61425007, Grant 61377090, Grant 61575128, Grant 61675137, and Grant 61505120; in part by the Guangdong Natural Science Foundation under Grant 2014A030308007, Grant 2014B050504010, Grant 2015B010105007, Grant 2015A030313541, and Grant 2015A030310243; in part by the Science and Technology Innovation Commission of Shenzhen under Grant GJHZ20150313093755757, Grant JCYJ20150324141711576, Grant JCYJ20160520163134575, Grant JCYJ20160427104925452, and Grant JCYJ20150324414171611; and in part by the Pearl River Scholar Fellowships. *(Zhiyong Bai and Mi Deng contributed equally to this work.)* Corresponding author: Yiping Wang (e-mail: ypwang@szu.edu.cn).

**Abstract:** We demonstrate a torsion sensor with rotation direction discrimination based on a pre-twisted core-cladding mode Mach–Zehnder interferometer (MZI) fabricated in single mode fiber by twisting the fiber during $CO_2$ laser irradiation to induce a permanent screw-type distortion at the two points of coupling between the core and cladding. The proposed sensor can measure the twist rate with a sensitivity of up to 10.35 nm/(rad/cm) and determine its rotation direction (i.e., clockwise or counterclockwise) simultaneously. Furthermore, the sensitivity of the torsion sensor can be enhanced by increasing the initial shear strain.

**Index Terms:** Fiber optics, fiber optics sensors, fiber optics components.

## 1. Introduction

Torsion sensors are of importance for measuring the twist of a structure owing to the application of an external torque, and have been widely used in scientific research and industry. Due to the unique advantages of optical fibers, numerous torsion sensors based on $CO_2$ laser inscribed long period fiber gratings (LPFGs) [1]–[3] and fiber Bragg gratings [4], [5] have been fabricated and have employed special fibers such as highly birefringence photonic crystal fibers, polarization maintaining fibers, and twin-core fibers [6]–[9]. However, some of these sensors cannot distinguish between applied torsions in the clockwise and counterclockwise directions. Although the $CO_2$ laser-inscribed LPFGs have been reported to demonstrate a degree of direction dependence owing to asymmetric exposure on the fiber cross-section, the reported torsion sensitivity was very low [1]. Recently, LPFGs with a helical structure have demonstrated a relatively high torsion sensitivity and good direction discrimination; however, the fabrication process is overly complex and cannot ensure a uniform helical grating modulation [10]–[13]. Alternatively, Mach-Zehnder interferometers (MZIs) based on optical fiber have been widely employed as refractive index sensors [14], temperature

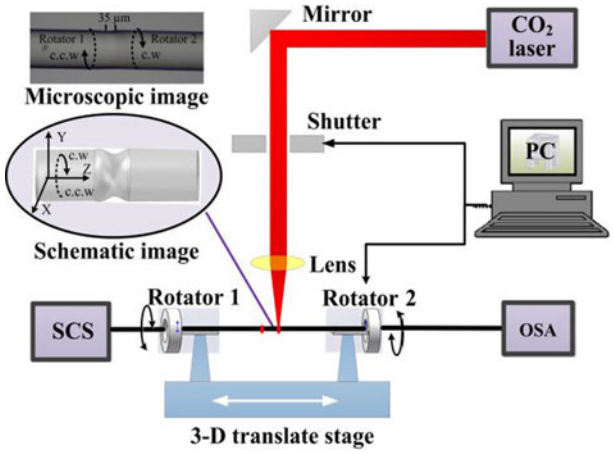


Fig. 1. Schematic illustration of the experimental setup employed for PT-MZI fabrication. The main components of the system consist of a $CO_2$ laser, a 3-D translation stage, and two rotators. The operations of the shutter and rotators are coordinated. A super-continuum light source (SCS) and an optical spectrum analyzer (OSA) were employed to monitor the transmission spectrum throughout the fabrication process. The microscopic image shows one of the screw-type deformations of the PT-MZI with fabrication parameters $\theta = \pi/2$ (for each rotator) and $v = 5^\circ/\text{s}$. The c.w. and c.c.w. marked in schematic image represent torsion direction of clockwise and counterclockwise, respectively.

sensors [15], and curvature sensors [16]. In addition to these sensors, torsion sensors based on MZIs or MZI-like devices have been recently reported. These include torsion sensors employing an MZI constructed by cascading two identical LPFGs [17], multimode interference based on square coreless fiber [18], and a dual polarized MZI composed of a sensor component and a demodulator [19]. These MZI-based torsion sensors demonstrate either good torsion sensitivity or direction discrimination, but a relative complex structure.

In this letter, we propose a novel pre-twisted in-fiber MZI (PT-MZI) that can measure the twist rate and determine the direction of rotation (clockwise or counterclockwise) simultaneously. The proposed PT-MZI was achieved by pre-twisting a conventional single mode fiber (SMF; Corning SMF-28e+) with core and cladding diameters of 8.2 $\mu$m and 125 $\mu$m, respectively, under $CO_2$ laser beam irradiation applied at the two points of coupling between the core and cladding modes, which creates a permanent shear strain in the fiber owing to an induced screw-type fiber deformation. Several PT-MZIs were fabricated, and their transmission spectra and torsion sensing characteristics were investigated experimentally. Under a permanent shear strain induced by pre-twisting, a shift in the interference fringe is observed relative to the interference fringe of an otherwise equivalent MZI without pre-twisting. As a result, the PT-MZI obtains an improved sensitivity of up to 10.35 nm/(rad/cm). When the direction of the applied torsion changes, the interference fringe of the PT-MZI shifts in the opposite direction. Moreover, the permanent shear strain in the PT-MZI has no obvious effect on the temperature response of the sensor.

## 2. Fabrication Method

The fabrication system for the proposed PT-MZI is presented schematically in Fig. 1. The main components of the system consisted of an industrial $CO_2$ laser (SYNRAD 48-1) with a maximum power of 10 W and a power stability of $\pm$2%, a 3-D translation stage with a repeatable accuracy of 80 nm, and a pair of rotators (Elliot Scientific MDE235) with a high rotation precision of 1 arcsecond (i.e., 1"). A custom computer program was developed with an easy-to-use operational interface to control the shutter and rotators. A super-continuum light source (SCS; NKT Photonics SuperK Compact) and an optical spectrum analyzer (OSA; YOKO-GAWA AQ6370C) were employed to monitor the transmission spectrum throughout the fabrication process.

Usually, a fiber inline Mach-Zehnder-type core-cladding mode interferometer is fabricated by machining micro-notches at two points of a SMF using continuous $CO_2$ laser irradiation to induce efficient light coupling between the core mode and the lower-order cladding modes [14]. To fabricate the PT-MZI, we introduce a preexisting shear strain in the SMF by twisting the fiber ends an amount $\theta$ (rad) in opposite directions using the two rotators. The shear strain is then frozen into the fiber at the two laser exposure points. The detailed fabrication of the PT-MZI is performed as follows. First, a bare section of the SMF is held in moderate tension by fiber holders fixed on the rotators, and the center of the bare section is positioned at the focal point of the $CO_2$ laser, which is only about 35 $\mu$m in diameter. Second, the shutter controlling the $CO_2$ laser and the two rotators are activated simultaneously. It is noted that the exposure time is related to both $\theta$ and the rotational velocity $v$ to ensure that the shutter is closed when the rotators stop. We note that $CO_2$ laser irradiation both couples the core and cladding and induces a permanent screw-type deformation over a very short segment of the fiber at the fusion point approximately equivalent to the focused spot diameter of the laser (i.e., 35 $\mu$m) [11], and the screw-type deformation can be either clockwise (C.W) or counterclockwise (C.C.W) depending on the sense of rotation, as illustrated by the microscopic and schematic images presented as insets in Fig. 1. Finally, the 3-D translation stage is moved by a desired length $L$, and the process is repeated at the new position. In this fabrication system, the separation between the two rotators was 5.5 cm, and thus, the frozen shear strain can be quantified by twist rate $\tau_0 = 2\theta/5.5 \approx 0.36\theta$ (rad/cm).

## 3. Operation Principle

When light is transmitted through the PT-MZI, part of the light energy in the fiber core will be coupled into the cladding through the first screw-type deformation point, which forms a mode splitter, while the second screw-type deformation point, which forms a mode combiner, will couple most of the cladding mode energy back into the core after passing through the section of fiber between the two fusion points, where part of the energy is attenuated due to cladding mode propagation. The propagation constants between core and cladding modes are different, such that the modes propagate at different speeds. Thus, the modes accumulate a phase difference as they propagate over the intermediary section of the fiber. The transmission of the PT-MZI can be expressed as a two-mode interferometer [14].

$$I = I_{co} + I_{cl} + 2\sqrt{I_{co} I_{cl}}\cos(\varphi). \tag{1}$$

Here, $I_{co}$ and $I_{cl}$ are the intensities of light guided in the core and cladding modes, respectively, and $\varphi = (2\pi\Delta n_{eff} L_0)/\lambda$ is the phase difference between the two light paths, where $\lambda$ is the operational wavelength, $L_0$ is the interference length which is approximately equal to $L$, and $\Delta n_{eff}$ is the difference between the effective refractive indices of the core $n_{eff}^{co}$ and cladding $n_{eff}^{cl}$ modes, and can be expressed as $\Delta n_{eff} = n_{eff}^{co} - n_{eff}^{cl}$.When the phase difference $\varphi = (2m+1)\pi$, $m = 0, 1, 2, ....$, the transmission dips occurs at

$$\lambda_m = \frac{2L\,\Delta n_{eff}}{2m\ +\ 1} \tag{2}$$

where $\lambda_m$ refers to the central wavelength of the mth order interference dip. The interference fringe spacing between adjacent interference notches (free spectral range, FSR) can be approximately by $FSR \approx \lambda_m^2/(\Delta n_{eff} L)$. Fig. 2(a) shows the FSR of MZI samples with different interference length $L$. The PT-MZI sensor can be achieved by monitoring the wavelength shift of the transmission dip $\lambda_m$ in response to external variables.

When the PT-MZI sample is subjected to torsion strain, according to (2) and ignoring the variable of $L$, the wavelength shift $\Delta\lambda_m$ can be derived as

$$\Delta\lambda_m \approx \lambda_m \frac{\delta\Delta n_{eff}}{\Delta n_{eff}} \tag{3}$$

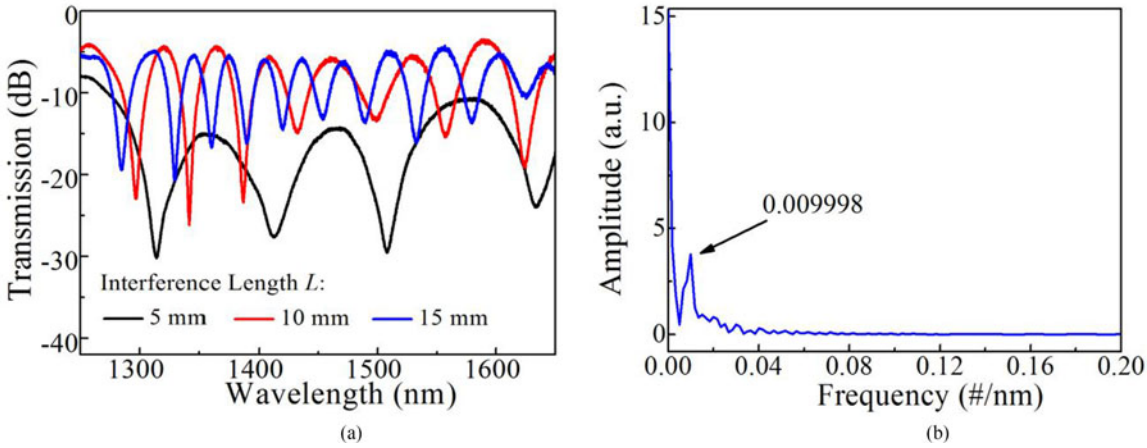


Fig. 2. (a) Transmission spectra of PT-MZI samples with $L = 5$, 10, and 15 mm under $\tau_0 = 0.57$ rad/cm. (b) FFT analysis of PT-MZI with $\tau_0 = 0.57$ rad/cm and $L = 5$ mm.

where,$\delta\Delta n_{eff}$ is the variable of $\Delta n_{eff}$, which is induced by the birefringence resulting from the photoelastic effect. $\delta\Delta n_{eff}$ in response to twist rate $\tau$ can be expressed as $\delta\Delta n_{eff} = (g^{co} n_{eff}^{co} - g^{cl} n_{eff}^{cl})\tau$, here, $g^{co}$ and $g^{cl}$ are the photoelastic constants for fiber core and cladding material, respectively. Therefore, the relationship between $\Delta\lambda_m$ and $\tau$ can be immediately obtained.

$$\Delta\lambda_m = \frac{\lambda_m}{\Delta n_{eff}} \left(g^{co} n_{eff}^{co} - g^{cl} n_{eff}^{cl}\right) \tau. \tag{4}$$

From (4), the term of $\lambda_m(g^{co} n_{eff}^{co} - g^{cl} n_{eff}^{cl})/\Delta n_{eff}$ is a wavelength-independent constant, and thus, the wavelength shift $\Delta\lambda_m$ is linearly proportional to the twist rate $\tau$.

For the $CO_2$ laser-based fabrication of a conventional MZI without pre-twisting [14], the responses of interference fringe to twist strain in the direction of c.w and c.c.w are similar due to the transverse symmetry on both side of the fiber notch. Thus, it cannot tell the torsion direction for this kind of MZI sensor. It is noted that the slopes of $\Delta\lambda_m$ to $\tau$ will not be the same for each torsion direction, because the evolution of birefringence may be different during twisting the fiber. However, for the PT-MZI, a permanent shear strain, and, hence, a permanent $\delta\Delta n_{eff}$ are induced and added to the original transmission spectrum. When an increasing shear strain is applied to the PT-MZI in a single direction, $\delta\Delta n_{eff}$ will be enhanced or impaired according to the direction of the applied torsion, which can be monitored by tracking the magnitude of the interference fringe shift and its direction. Therefore, the PT-MZI can determine the twist direction and measure the twist rate simultaneously.

## 4. Characteristics of Transmission Spectra

We first investigated the characteristics of the transmission spectra obtained from the proposed PT-MZI sensor. To this end, several PT-MZI samples with different values for parameter $L$ and $\tau_0$ were fabricated, and their screw-type deformation is set to be clockwise. Fig. 2(a) shows the transmission spectra of three different PT-MZI samples with equivalent values of $\tau_0 = 0.57$ rad/m, corresponding to $\theta = \pi/2$ for each rotator, and different values of $L = 5$, 10, and 15 mm. we can see from Fig. 2(a) that the transmission spectra of the PT-MZI sensors are dependent on $L$. Here, the separation between two adjacent interference fringes is observed to decrease in an approximately inverse proportion to $L$, which corresponds with core-cladding mode interference theory. A fast Fourier transform is operated on the transmission spectrum of PT-MZI with $\tau_0 = 0.57$ rad/cm and $L = 5$ mm to offer a deep sight into the mode components involved in the interference process as shown in Fig. 2(b). Obviously, the transmission spectrum is mainly induced by two modes interaction.

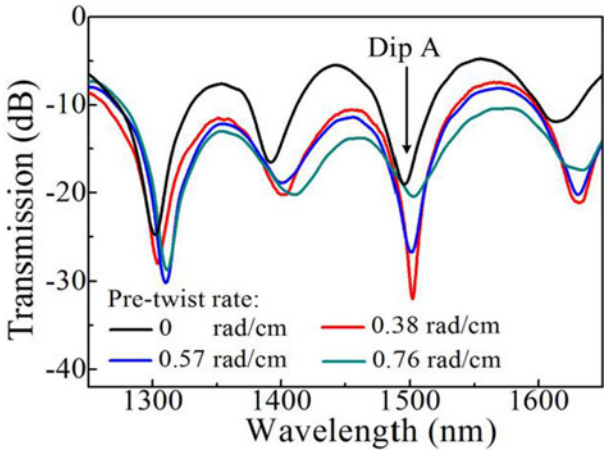


Fig. 3. Transmission spectra of PT-MZI samples with a constant $L = 5$ mm and with $\tau_0 = 0$ (MZI-1), 0.38 (MZI-2), 0.57 (MZI-3), and 0.76 (MZI-4) rad/cm (corresponding to $\theta = 0$, $\pi/3$, $\pi/2$, and $2\pi/3$, respectively, for each rotator). Dip A serves as the interference fringe of interest in the remaining discussion.

Fig. 3 shows the transmission spectra of four PT-MZI samples with a constant $L = 5$ mm and with different $\tau_0 = 0$, 0.38, 0.57, and 0.76 rad/m corresponding to different $\theta = 0$, $\pi/3$, $\pi/2$, and $2\pi/3$ for each rotator, which are denoted here in as MZI-1 (i.e., a conventional fiber-based MZI with $\tau_0 = 0$ rad/cm for comparison), MZI-2, MZI-3, and MZI-4, respectively. we can see that the value of $\tau_0$ has an effect on the transmission spectra as well, where the interference fringes associated with Dip A undergo a shift due to the different values of $\delta\Delta n_{eff}$ induced by pre-twisting.

## 5. Sensing Characteristic

To investigate the effect of an applied torsion on the transmission spectra of the proposed PT-MZI, torsion tests were conducted with the four PT-MZI samples with equivalent $L'$ using the rotation and monitoring apparatus shown in Fig. 1. Here, the $L'$ is equal to the distance between two fiber holders and hence $L' = 5.5$ cm; thus, the applied torsion $\tau = \beta/L' = \beta/5.5 \approx 0.18\beta$ rad/cm, where $\beta$ is applied angle. Experimentally, we fixed rotator 1, and only rotated rotator 2 in clockwise $(+)$ or counterclockwise $(-)$ directions with rotation angles $\beta$ varying from $-2\pi$ to $2\pi$ in intervals of $\pi/2$. The transmission spectra of the PT-MZI samples were recorded, and the wavelength shifts were measured by tracking Dip A. As can be observed in Fig. 4(a), the sample MZI-1 fabricated without pre-twisting exhibits an interference fringe shift that is independent of the torque direction, as indicated by shifting towards smaller wavelengths with the application of both clockwise and counterclockwise torsions. Meanwhile, the torsional characteristics of MZI-2, MZI-3, and MZI-4, which can be seen in Fig. 4(b)–(d), respectively, present reliable direction dependence, as indicated by the wavelength shifts exhibiting an opposite response to the application of clockwise and counterclockwise torsions, corresponding to a red shift and blue shift, respectively.

The wavelength shifts of Dip A for the four PT-MZI samples are plotted in Fig. 5. An approximately linear relationship is observed between the wavelength shift and the applied torsion in the clockwise and counterclockwise directions. Therefore, the data was subjected to linear fitting, and the slopes, indicative of the torsion sensitivities of the four PT-MZI samples, are listed in Table 1. This shows that increasing $\tau_0$ increases the torsion sensitivity, particularly for clockwise torsion. We note that, with $\tau_0$ increased from 0.38 rad/cm to 0.76 rad/cm, the torsion sensitivity increased from $+2.05$ nm/(rad/cm) to $+10.35$ nm/(rad/cm) for clockwise torsion, and increased from $-2.05$ nm/(rad/cm) to $-3.65$ nm/(rad/cm) for counterclockwise torsion, where positive values represent a red shift and negative values represent a blue shift.

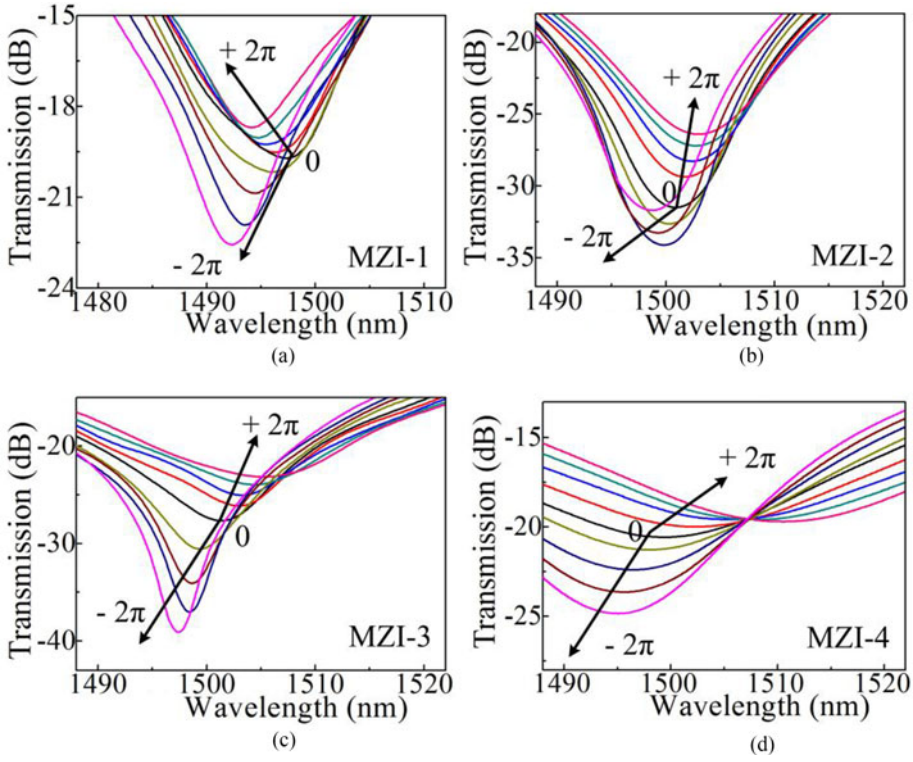


Fig. 4. Transmission spectra evolutions of Dip A under torsion applied with clockwise (+) and counterclockwise (−) rotations from $-2\pi$ to $2\pi$ in intervals of $\pi/2$ for (a) MZI-1 ($\tau_0 = 0$ rad/cm), (b) MZI-2 ($\tau_0 = 0.38$ rad/cm), (c) MZI-3 ($\tau_0 = 0.57$ rad/cm), and (d) MZI-4 ($\tau_0 = 0.76$ rad/cm).

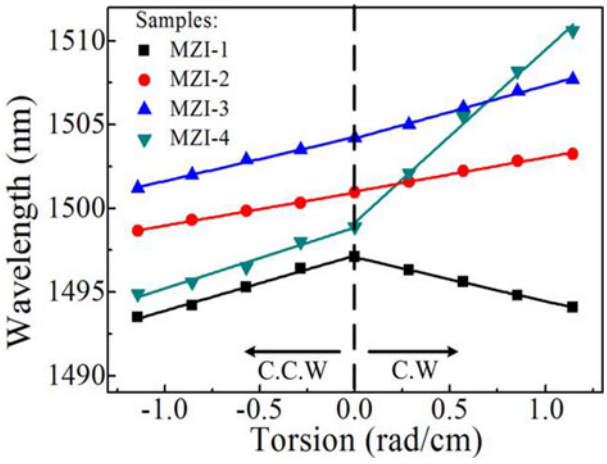


Fig. 5. Linear fitting of the wavelength shifts of Dip A shown in Fig. 4 with C.W. and C.C.W. rotations.

The temperature behavior of the four PT-MZI samples was also investigated to determine if the pre-twisting had an effect on the temperature response of the proposed PT-MZI. The samples were heated in an electric furnace from 30 °C to 100 °C in air with 10 °C steps. The evolution of Dip A is shown in Fig. 6. The wavelength shift data was plotted with respect to temperature in Fig. 7, and subjected to linear fitting. It can be seen that the temperature dependence of the wavelength shift of Dip A was roughly linear for all four PT-MZI samples and that all samples presented an equivalent temperature response, as indicated by the slopes of the lines (given in the chart legend).

TABLE 1
Torsion Sensitivity of PT-MZIs

| Samples | $\theta^*$ | $\tau_0$ (rad/cm) | $S_{c.w}$ (nm/rad/cm) | $S_{c.c.w}$ (nm/rad/cm) |
|---|---|---|---|---|
| MZI-1 | 0 | 0 | −2.62 | −3.29 |
| MZI-2 | $\pi/3$ | 0.38 | +2.04 | −1.97 |
| MZI-3 | $\pi/2$ | 0.57 | +3.15 | −2.63 |
| MZI-4 | $2\pi/3$ | 0.76 | +10.32 | −3.64 |

$*$ For each rotator. $S_{c.w}$ and $S_{c.c.w}$ represent the torsion sensitivity in the direction of c.w and c.c.w, respectively.

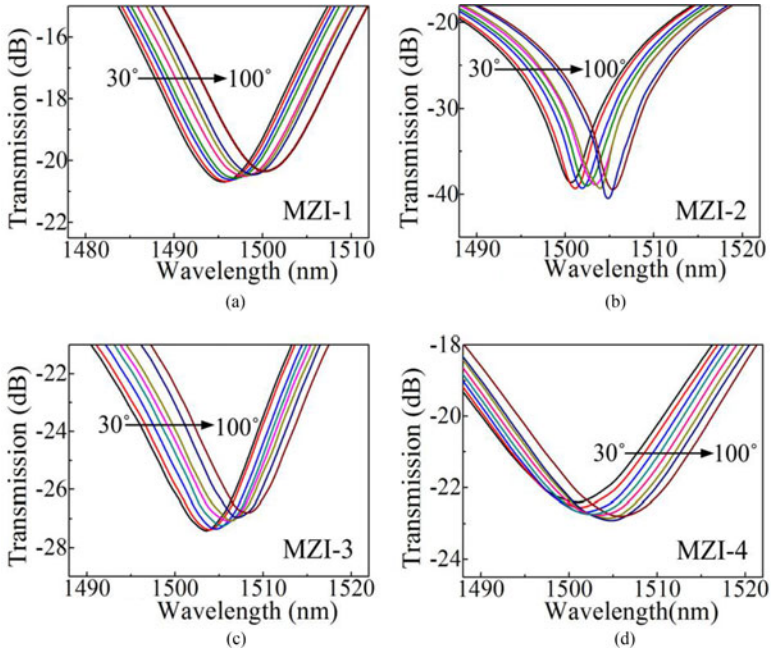


Fig. 6. Transmission spectra evolutions of Dip A with increasing temperature from 30 °C to 100 °C for (a) MZI-1, (b) MZI-2, (c) MZI-3, and (d) MZI-4.

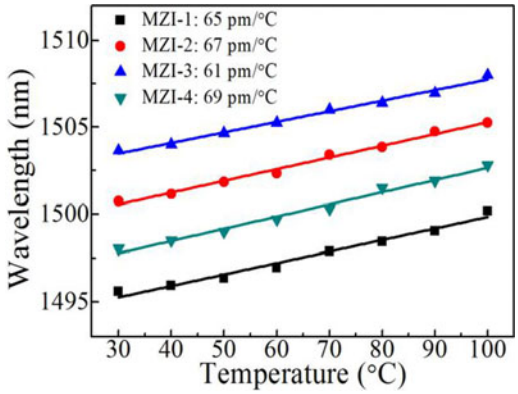


Fig. 7. Linear fitting of the wavelength shifts of Dip A with temperature increasing from 30 °C to 100 °C

This demonstrates that pre-twisting had no effect on the temperature response of the proposed PT-MZI.

## 6. Conclusion

We have proposed a novel pre-twisted core-cladding mode MZI fabricated in SMF by pre-twisting the fiber during $CO_2$ laser exposure to induce a permanent screw-type distortion at the points of coupling between the core and cladding modes. The influence of the initial shear strain on the torsion and temperature dependence properties of the PT-MZI was investigated in detail. It was shown experimentally that including a permanent shear strain in the MZI facilitated good torsion direction discrimination based on the direction of the shift in the interference fringe. In addition, increasing the preexisting shear strain from 0.38 rad/cm to 076 rad/cm significantly enhanced the torsion sensitivity from $+2.05$ nm/(rad/cm) to $+10.35$ nm/(rad/cm) for the clockwise application of torsion and moderately enhanced the torsion sensitivity from $-2.05$ nm/(rad/cm) to $-3.65$ nm/(rad/cm) for the counterclockwise application of torsion. Furthermore, the preexisting shear strain has a negligible influence on the temperature sensitivity of the proposed PT-MZI in the temperature range of 30 °C to 100 °C.

## References


[1] Y. P. Wang and Y. J. Rao, "Long period fibre grating torsion sensor measuring twist rate and determining twist direction simultaneously," *Electron. Lett.*, vol. 40, pp. 164–166, 2004.

[2] Y. P. Wang, J. P. Chen, and Y. J. Rao, "$CO_2$-laser induced LPFG's torsion characteristics depending on the length of the twisted fiber," *Amer. J. Addictions*, vol. 9, pp. 94–95, 2000.

[3] Y. J. Rao, T. Zhu, and Q. J. Mo, "Highly sensitive fiber-optic torsion sensor based on an ultra-long-period fiber grating," *Opt. Commun.*, vol. 266, pp. 187–190, 2006.

[4] W. Yiping, M. Wang, and X. Huang, "In fiber Bragg grating twist sensor based on analysis of polarization dependent loss," *Opt. Exp.*, vol. 21, pp. 11913–11920, 2013.

[5] J. Wo *et al.*, "Twist sensor based on axial strain insensitive distributed bragg reflector fiber laser," *Opt. Exp.*, vol. 20, pp. 2844–2850, 2012.

[6] O. Frazão, R. M. Silva, J. Kobelke, and K. Schuster, "Temperature- and strain-independent torsion sensor using a fiber loop mirror based on suspended twin-core fiber," *Opt. Lett.*, vol. 35, pp. 2777–2779, 2010.

[7] H. M. Kim, T. H. Kim, B. Kim, and Y. Chung, "Temperature-insensitive torsion sensor with enhanced sensitivity by use of a highly birefringent photonic crystal fiber," *IEEE Photon. Technol. Lett.*, vol. 22, no. 20, pp. 1539–1541, Oct. 2010.

[8] P. Zu, C. C. Chan, Y. Jin, and T. Gong, "A temperature-insensitive twist sensor by using low-birefringence photonic-crystal-fiber-based sagnac interferometer," *IEEE Photon. Technol. Lett.*, vol. 23, no. 13, pp. 920–922, Jul. 2011.

[9] B. Song *et al.*, "Highly sensitive twist sensor employing Sagnac interferometer based on PM-elliptical core fibers," *Opt. Exp.*, vol. 23, pp. 15372–15379, 2015.

[10] R. Gao, Y. Jiang, and L. Jiang, "Multi-phase-shifted helical long period fiber grating based temperature-insensitive optical twist sensor," *Opt. Exp.*, vol. 22, pp. 15697–15709, 2014.

[11] S. Oh, K. R. Lee, U. C. Paek, and Y. Chung, "Fabrication of helical long-period fiber gratings by use of a $CO_2$ laser," *Opt. Lett.*, vol. 29, pp. 1464–1466, 2004.

[12] W. Shin, B. A. Yu, Y. L. Lee, Y. C. Noh, D. K. Ko, and J. Lee, "High strength coupling and low polarization-dependent long-period fiber gratings based on the helicoidal structure," *Opt. Fiber Technol.*, vol. 14, pp. 323–327, 2008.

[13] L. Zhang, Y. Liu, Y. Zhao, and T. Wang, "High sensitivity twist sensor based on helical long-period grating written in two-mode fiber," *IEEE Photon. Technol. Lett.*, vol. 28, no. 15, pp. 1629–1632, Aug. 2016.

[14] T. Wei, X. Lan, and H. Xiao, "Fiber Inline core–cladding-mode Mach–Zehnder interferometer fabricated by two-point $CO_2$ laser irradiations," *IEEE Photon. Technol. Lett.*, vol. 21, no. 10, pp. 669–671, Jun. 2009.

[15] J. Zhou *et al.*, "Simultaneous measurement of strain and temperature by employing fiber Mach-Zehnder interferometer," *Opt. Exp.*, vol. 22, pp. 1680–1686, 2014.

[16] O. Frazão *et al.*, "All-fiber Mach-Zehnder curvature sensor based on multimode interference combined with a long-period grating," *Opt. Lett.*, vol. 32, pp. 3074–3076, 2007.

[17] L. Shi, T. Zhu, Y. E. Fan, K. S. Chiang, and Y. Rao, "Torsion sensing with a fiber ring laser incorporating a pair of rotary long-period fiber gratings," *Opt. Commun.*, vol. 284, pp. 5299–5302, 2011.

[18] B. Song, Y. Miao, W. Lin, H. Zhang, J. Wu, and B. Liu, "Multi-mode interferometer-based twist sensor with low temperature sensitivity employing square coreless fibers," *Opt. Exp.*, vol. 21, pp. 26806–26811, 2013.

[19] L. Chen *et al.*, "In-fiber torsion sensor based on dual polarized Mach-Zehnder interference," *Opt. Exp.*, vol. 22, pp. 31654–31664, 2014.